A three-dimensional vessel-on-chip model to study Puumala orthohantavirus pathogenesis

Noack, D.; Haperen, A. van; Hout, M.C.G.N. van den; Marshall, E.M.; Koutstaal, R.W.; Duinen, V. van; ... ; Rockx, B.

Lab on a Chip

PAPER

View Article Online
View Journal | View Issue

Cite this: *Lab Chip*, 2024, **24**, 5347

A three-dimensional vessel-on-chip model to study Puumala orthohantavirus pathogenesis†

Danny Noack,[a] Anouk van Haperen,[a] Mirjam C. G. N. van den Hout,[bc] Eleanor M. Marshall,[a] Rosanne W. Koutstaal,[a] Vincent van Duinen,[d] Lisa Bauer,[a] Anton Jan van Zonneveld,[d] Wilfred F. J. van IJcken,[bc] Marion P. G. Koopmans[a] and Barry Rockx*[a]

Received 26th June 2024,
Accepted 27th August 2024

DOI: 10.1039/d4lc00543k

rsc.li/loc

Puumala orthohantavirus (PUUV) infection in humans can result in hemorrhagic fever with renal syndrome. Endothelial cells (ECs) are primarily infected with increased vascular permeability as a central aspect of pathogenesis. Historically, most studies included ECs cultured under static two-dimensional (2D) conditions, thereby not recapitulating the physiological environment due to their lack of flow and inherent pro-inflammatory state. Here, we present a high-throughput model for culturing primary human umbilical vein ECs in 3D vessels-on-chip in which we compared host responses of these ECs to those of static 2D-cultured ECs on a transcriptional level. The phenotype of ECs in vessels-on-chip more closely resembled the *in vivo* situation due to higher similarity in expression of genes encoding described markers for disease severity and coagulopathy, including *IDO1*, *LGALS3BP*, *IL6* and *PLAT*, and more diverse endothelial-leukocyte interactions in the context of PUUV infection. In these vessels-on-chip, PUUV infection did not directly increase vascular permeability, but increased monocyte adhesion. This platform can be used for studying pathogenesis and assessment of possible therapeutics for other endotheliotropic viruses even in high biocontainment facilities.

Introduction

Orthohantaviruses are emerging zoonotic viruses able to cause severe disease in humans. These viruses are wide-spread over the globe as each orthohantavirus is maintained in a specific reservoir animal species, mostly rodents. Following inhalation of contaminated aerosols, Puumala orthohantavirus (PUUV) can cause a mild form of hemorrhagic fever with renal syndrome (HFRS) in humans, named *nephropathia epidemica* (NE). NE is characterized by fever, altered coagulation, thrombocytopenia and acute kidney injury (AKI). The primary target cells of pathogenic orthohantavirus infection are endothelial cells (ECs) of different organs, which play a central role in pathogenesis.[1] Previous *in vitro* studies have primarily focused on the effects of EC infection by other orthohantaviruses, such as Hantaan orthohantavirus (HTNV) and Andes orthohantavirus (ANDV), resulting in increased vascular permeability with a central role for adherens junction protein VE-cadherin.[2–5] However, vascular permeability and EC responses in the context of PUUV infection are less well understood.

Historically, most studies have relied on *in vitro* models in which ECs are cultured as flat monolayers that do not form a three-dimensional (3D) tube-like architecture that interacts with an extracellular matrix (ECM) like in normal *in vivo* vasculature, and do not experience physiologically relevant flow-induced shear stress, *i.e.* static two-dimensional (2D) cultures. However, it is known that by culturing ECs in this manner, their morphology, proliferation rate and gene expression profiles are altered compared to their *in vivo* phenotype.[6,7] More specifically, the lack of physiologically relevant flow primes ECs to a more pro-inflammatory phenotype[6,8] whilst the presence of prolonged flow is more crucial in mimicking the original *in vivo* EC transcriptomic signature than for instance co-culturing with relevant neighboring cells such as smooth muscle cells.[7]

So, there is a clear unmet need for a physiologically relevant 3D EC culture model that includes flow-induced shear stress, and provides opportunities to study important EC functions such as vascular barrier function and the interplay between blood compartments, including leukocytes, in the context of

[a] *Department of Viroscience, Erasmus University Medical Center, s-Gravendijkwal 230, 3015 CE, Rotterdam, the Netherlands. E-mail: b.rockx@erasmusmc.nl*
[b] *Department of Cell Biology, Erasmus University Medical Center, Rotterdam, the Netherlands*
[c] *Center for Biomics, Erasmus University Medical Center, Rotterdam, the Netherlands*
[d] *Department of Internal Medicine, Division of Nephrology and the Einthoven Laboratory for Vascular and Regenerative Medicine, Leiden University Medical Center, Leiden, the Netherlands*

† Electronic supplementary information (ESI) available. See DOI: https://doi.org/10.1039/d4lc00543k

orthohantavirus infection. Many of such vessel-on-chip devices have been described that allow for recapitulation of functional human vascular structures to study certain aspects of angiogenesis[9–13] or thrombosis.[10,14,15] However, most of these models rely on specialized equipment such as pump systems or do not yet facilitate high-throughput usage by their limited reproducibility, thereby restricting their potential to study virus infections in high-containment settings. Here, we present a high-throughput microfluidics platform in which primary ECs form 3D vessels-on-chip that are exposed to flow. We chose to use PUUV as model pathogen, as little is known about the effects of PUUV infection on vascular permeability and can be handled at biosafety level 2 (BSL-2), unlike some of the other human pathogenic orthohantaviruses, such as HTNV and ANDV.

This study demonstrates the added value of vessel-on-chip cultures compared to static 2D cultures by identifying that ECs in vessels-on-chip more closely resemble *in vivo* responses as characterized by an increased similarity of expression of disease severity and coagulopathy markers, as observed in PUUV patients, and more diverse endothelial-leukocyte crosstalk as response to PUUV infection. This model represents a valuable high-throughput platform to study viral pathogenesis in 3D vessels.

Results

Reproducible 3D vessels-on-chip can be used up to two weeks and respond less inflammatory to tumor necrosis factor alpha compared to static 2D EC cultures

To establish a physiologically relevant model for ECs, a previously developed flow-based 3D vessel-on-chip platform was used.[16] In short, microfluidic chips are integrated

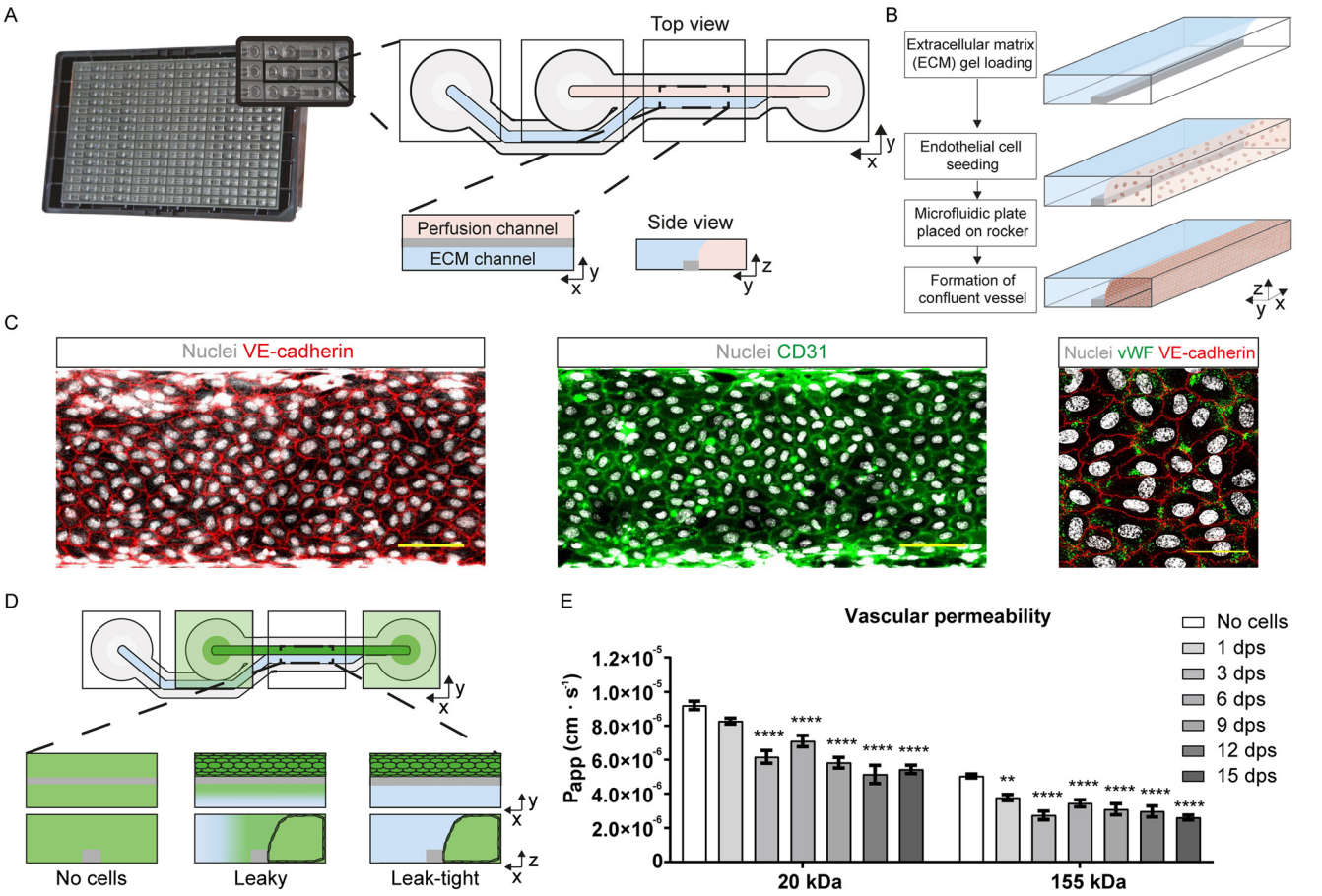

Fig. 1 Establishment of three-dimensional perfused vessels-on-chip. (A) Schematic representation of each independent chip. A chip is composed of four adjacent wells beneath a 384-wells plate which includes two channels; an extracellular matrix (ECM; in blue) and perfusion channel (in pink). The two channels intersect below each third well, which facilitates confocal imaging. (B) An ECM gel is loaded into the gel inlet well and allowed to polymerize for at least two days. ECs are seeded into the perfusion channel and allowed to adhere to the bottom of the perfusion channel. After adherence, the microfluidic plate is placed onto an interval rocker facilitating gravity-based flow and perfusion of the ECs, allowing for the formation of confluent three-dimensional (3D) vessels-on-chip. (C) Representative immunofluorescence images of vessels-on-chip that were stained for EC markers VE-cadherin (red), CD31 (green) and Von Willebrand factor (vWF; green). Nuclei are shown in white. Scale bars for VE-cadherin and CD31 images represent 100 μm, scale bar for vWF staining represents 50 μm. (D) Schematic representation of the vascular permeability assay in which EC culture medium is replaced with medium containing fluorescently labeled dextran reporters of different sizes. (E) Translocation of fluorescently-labeled 20 and 155 kDa dextran reporters from the perfusion channel into the ECM channel was quantified to result in the apparent permeability (P_{app}). P_{app} values at different time points post-seeding (dps) were compared to the maximum P_{app}, which was defined by translocation towards the ECM gel in absence of cells (no cells), by two-way ANOVA with Dunnett's correction. Results were combined from three independent experiments for 20 kDa (N = 13–22 vessels per time point) and four independent experiments for 155 kDa (N = 17–27 vessels per time point). $^{**}p < 0.005$, $^{****}p < 0.0001$.

underneath a 384-wells plate and each chip is positioned underneath four wells, which include one gel inlet well, one perfusion inlet well, one observation well and one perfusion outlet well (Fig. 1A). After loading and polymerization of a collagen-based ECM gel into an ECM channel (Fig. 1A), primary pooled human umbilical vein ECs (HUVECs) were seeded into a gelatin-coated perfusion channel (Fig. 1A) and allowed to adhere without the use of artificial membranes.[17,18] After adherence, the microfluidic plate was placed onto an interval rocker facilitating hydrostatic pressure-driven continuous bidirectional flow and perfusion of the ECs.[18] Within one day of culture, formation of confluent vessels against the ECM were consistently observed (Fig. 1B). The endothelial phenotype and integrity of the monolayers in these vessels were confirmed *via* immunofluorescence staining of endothelial-specific combination of markers such as VE-cadherin, CD31 and Von Willebrand factor (vWF) (Fig. 1C), which also allowed for the visualization of the 3D tube-like architecture and perfusable lumen of these vessels (Video S1†). Vascular barrier function was assessed by solute flux assay using fluorescently-labeled dextrans of different molecular weights (20 and 155 kDa), that, upon addition to the perfusion inlet and outlet wells, diffuse from the vessel lumen, located in the perfusion channel, into the adjacent ECM gel, located in the ECM channel[16,19] (Fig. 1D). Vascular permeability was defined as apparent permeability (P_{app}) and determined by quantifying translocation of fluorescently-labeled dextran reporters from the vessel lumen into the ECM gel over time. To determine on which days post-seeding (dps) the endothelial vessels-on-chip formed an optimal and stable barrier, the P_{app} was calculated on different dps and compared to the maximum P_{app} as represented by the intrinsic barrier of the ECM gel in absence of ECs, *i.e.* no cells. This resulted in a significant barrier formation for 20 kDa and 155 kDa from 3 dps until the end of the experiment at 15 dps (Fig. 1E).

To demonstrate the physiological relevance of the vessel-on-chip culture in context of a biological stimulus, bulk RNA-sequencing (RNA-Seq) was performed to characterize responses of ECs that were either cultured in vessels-on-chip or under static 2D conditions, *i.e.* in a 96-wells plate lacking flow, and in the presence or absence of tumor necrosis factor alpha (TNFα). TNFα represents an important driver of inflammatory responses in vascular ECs, resulting in various processes such as increased vascular permeability, immune cell recruitment and disturbed coagulation. RNA-Seq transcriptional profiles demonstrated that TNFα treatment resulted in significant changes in gene expressions with the majority, 644 upregulated and 523 downregulated genes, shared between ECs in both culturing methods (Fig. S1A–D†). Overall, a higher number of genes were differentially expressed following TNFα treatment in static 2D cultures (Fig. S1B†), and there was a trend of higher fold changes in static 2D cultures for common significantly upregulated genes (Fig. S1E†). Pathway enrichment analyses demonstrated that EC responses to TNFα treatment were generally comparable, however uniquely enriched pathways existed with increased cytokine signaling in the vessel-on-chip cultures and increased eosinophil chemotaxis, T cell activation and pattern recognition receptor activity in static 2D cultures (Fig. S1F†). Overall, these RNA-Seq data indicated that ECs cultured in vessels-on-chip, compared to static 2D cultures, demonstrated a less inflammatory response to a biological stimulus such as TNFα, which aligns with previous findings on pro- and anti-inflammatory bioactive lipids in response to TNFα in similar vessels-on-chip and static 2D EC cultures.[20] In line with these findings, it has previously been demonstrated that prolonged exposure to *in vivo*-like levels of flow-induced shear stress, protects against TNFα-induced pro-inflammatory responses both *ex vivo* and *in vitro*.[21,22] Altogether, vessel-on-chip culture allows for improved recapitulation of *in vivo* EC responses to biological stimuli such as TNFα.

PUUV follows similar replication kinetics in both EC culture models and does not directly lead to increased vascular permeability

To determine the translatability of the vessel-on-chip model in context of orthohantavirus infection, PUUV replication kinetics in both models were compared. The replication kinetics and infection rates of PUUV in vessels-on-chip and static 2D cultures were comparable with a peak of replication at 4 days post-infection (dpi; Fig. 2A). Infection rates were similar at 4 dpi, with the majority of the cells being infected (Fig. 2B). So, PUUV replication was similar in both culture models, which allowed for direct comparison of EC responses to PUUV infection in both models.

To assess the effect of PUUV infection on the vascular barrier function, VE-cadherin was stained and the vascular permeability was assessed. As additional control for requirement of active viral replication on the effects on vascular permeability, vessels-on-chip were inoculated with UV-inactivated PUUV (UV-PUUV). Although the positive control condition, TNFα treatment, clearly impacted the expression of VE-cadherin on the cells, PUUV did not significantly impact the expression of VE-cadherin in vessels-on-chip (Fig. 2B). Also, PUUV infection did not directly lead to vascular permeability increases compared to mock, *i.e.* vessels-on-chip that were inoculated with corresponding volume of Vero E6 cell culture medium diluted in EC culture medium as used during infections with infectious PUUV stock (Fig. 2C). In contrast, TNFα treatment did lead to significantly increased vascular permeability. UV-PUUV did not have significant effects on VE-cadherin expression or vascular permeability. Overall, PUUV replicated in a similar manner in vessels-on-chip compared to static 2D EC cultures and infection of ECs did not directly cause increased vascular permeability in vessels-on-chip.

Vessels-on-chip are more suitable for study of endothelial–leukocyte interactions during PUUV infection

As the vessel-on-chip represents a platform to study the effects of PUUV infection in physiologically relevant conditions, it provided the opportunity to characterize the

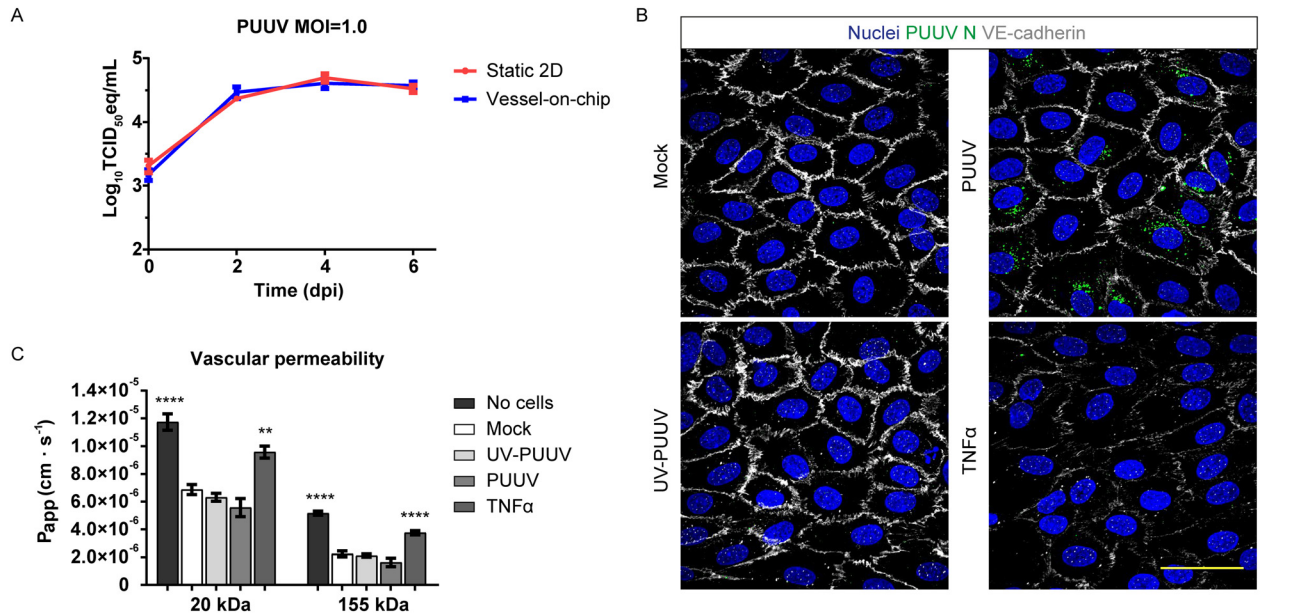

Fig. 2 PUUV replication kinetics and the effects on vascular permeability in vessels-on-chip. (A) PUUV replication kinetics in supernatants of ECs in static 2D or vessel-on-chip cultures. Samples were taken every two days after initial infection with MOI of 1.0. Squares and dots indicate the mean $TCID_{50}$ equivalents (eq.) per mL and error bars indicate standard error of the mean. Results are combined from three independent experiments with each 3 wells or chips per condition. (B) Representative images of immunofluorescence staining for PUUV N and VE-cadherin in mock-, UV-inactivated PUUV (UV-PUUV)-, PUUV- and TNFα-treated vessels-on-chip at 4 days post-infection (dpi). Images are representative for three independent experiments with each 3 wells or chips per condition. Scale bar represents 50 μm. (C) Vascular permeability is expressed as apparent permeability (P_{app}) for fluorescently-labeled 20 and 155 kDa dextran reporters. P_{app} values of a no cells control condition, UV-PUUV-, PUUV-, and TNFα-treated vessels-on-chip were compared to those values of mock-infected vessels-on-chip, *i.e.* vessels-on-chip inoculated with corresponding volume of Vero E6 cell culture medium diluted in EC culture medium as used during inoculations with infectious PUUV stock, at 4 dpi by one-way ANOVA with Dunnett's correction. Results are representative for two independent experiments with 6 vessels per condition. $^{**}p < 0.005$, $^{****}p < 0.0001$.

host response to PUUV. To compare EC responses to PUUV infection in both models, RNA-Seq was performed on mock- and PUUV-infected ECs at 4 dpi. The principal component analysis (PCA) plot displayed clustering of biological replicates with a profound transcriptomic shift in response to PUUV infection (Fig. 3A). PUUV infection resulted in more significantly upregulated genes compared to downregulated genes in both culturing platforms. In static 2D cultures, PUUV infection resulted in significant upregulation of 231 genes and downregulation of 175 genes, while in the vessels-on-chip more genes (297) were upregulated and approximately the same number of genes (172) were downregulated (Fig. 3B). PUUV infection resulted in 189 common upregulated genes and 89 common downregulated genes in ECs in both culture models (-Fig. 3B–D). Among these common upregulated genes were two known severity of disease markers for PUUV infection in human cases, namely *IDO1*, which encodes indoleamine 2, 3-dioxygenase (IDO),[23] and *LGALS3BP*, which encodes galectin-3-binding protein (Gal-3BP).[24] There was an increased expression of genes involved in the immune response such as *HLA-F*, *SAMD9*, *HLA-B*, genes encoding chemokines such as *CXCL10*, *CCL5*, *CXCL11*, genes encoding cell surface markers such as *LGALS9B*, *LGALS9*, *LY6E*, and genes involved in interferon (IFN) signaling such as *MX2*, *RSAD2* and *CMPK2* (Table 1). However, in addition to common genes, PUUV infection also led to the unique upregulation of 108 genes (36.4%) and unique downregulation of 83 genes (48.3%) in the vessels-on-chip, including upregulation of an additional marker of disease severity, *IL6*, encoding interleukin-6 (IL-6).[25,26] Other uniquely upregulated genes were involved in the immune response such as *NEURL3*, *C3AR1*, *NOD2*, genes encoding chemokines and cytokines such as *IL7*, *CCL23*, *IL15*, genes encoding cell surface markers such as *IL12RB1*, *CD7*, *IL7R* and genes involved in IFN signaling such as *IFNB1*, *IRF1* and *TRIM26* (Table 2). Additionally, significant upregulation of expression of genes associated to coagulopathy, as frequently observed in patients,[27,28] such as *PLAT*, *SERPINB2* and *SERPIND1*, was also observed. In contrast, unique gene expression upregulation was observed in static 2D cultures for *TLR6*, involved in the immune response, chemokines and cytokines encoding genes such as *CXCL5*, *EBI3*, *GDF7* and cell surface markers encoding genes such as *SELE*, *VCAM1* and *CD164*. No genes were significantly upregulated in vessels-on-chip and significantly downregulated in static 2D cultures or *vice versa*.

Next, enriched pathways in response to PUUV infection were identified in both culture models. In line with the gene expression profiles, there was an overlap in enriched pathways, which mainly consisted of (innate) immune and anti-viral defense responses (Fig. 3E). The top five unique

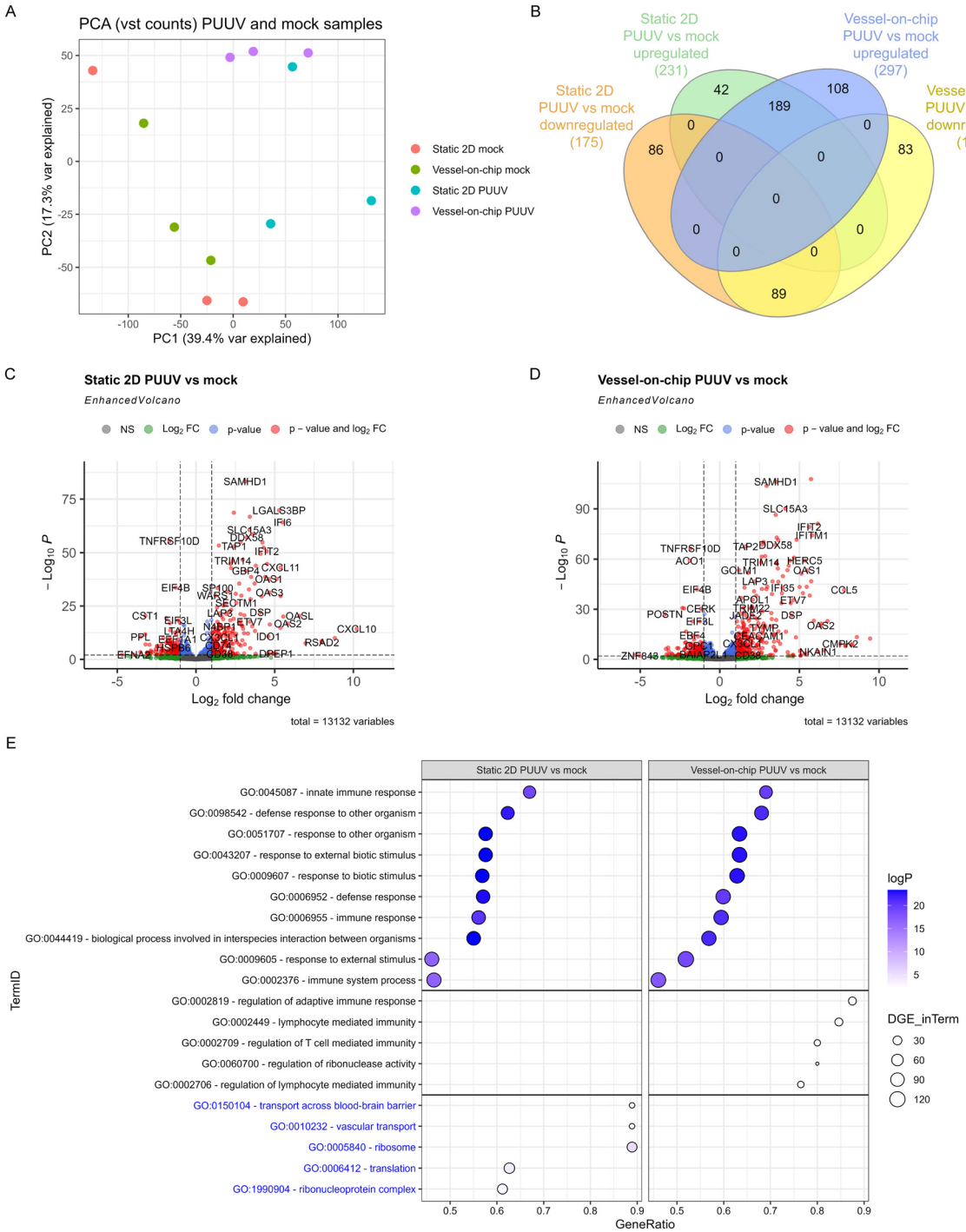

Fig. 3 RNA-Seq analyses of ECs cultured in static 2D and vessel-on-chip models upon PUUV infection. (A) Principal component analysis (PCA) plot based on vst normalized counts of mock- and PUUV-infected samples of static 2D and vessel-on-chip EC cultures at 4 days post-infection (dpi). (B) Venn diagram comparing significantly upregulated and downregulated genes in response to PUUV infection at 4 dpi in static 2D and vessel-on chip cultures. (C) Volcano plot demonstrating significantly upregulated and downregulated gene expressions following PUUV infection compared to mock-infected cells in static 2D-cultured ECs at 4 dpi. Grey dots represent genes which expressions neither significantly altered nor exceeded the fold change cut-off. Blue dots represent significantly altered genes that did not exceed the fold change cut-off. Green dots represent genes which expressions were not significantly altered, but exceeded the fold change cut-off. Red dots represent genes with significantly altered expressions that also exceeded the fold change cut-off. (D) Volcano plot demonstrating significantly upregulated and downregulated gene expressions following PUUV infection compared to mock-infected cells in vessel-on-chip-cultured ECs at 4 dpi. (E) PUUV-induced transcriptomic gene expression profile overview for ECs cultured in static 2D or vessels-on-chip. Balloon plot displaying significantly (Benjamini-Hochberg adjusted P-value < 0.05) enriched GO-terms upon PUUV infection at 4 dpi. Size of the balloon represents the number of differentially expressed genes within a GO-term (DGE_inTerm) while the color of the balloon represents the negative base-10 logarithm of the P-value. GeneRatio on the x-axis is the number of differentially expressed genes divided by the total number of genes involved in the GO-term. Significant GO-terms were ranked on highest GeneRatio, displaying the top 10 common pathways, and top 5 for unique pathways for vessel-on-chip and static 2D cultures. Blue font indicates that the enrichment of the GO-term was mainly based on downregulated genes.

Table 1 Common significantly upregulated genes upon PUUV infection in static 2D- and vessel-on-chip-cultured ECs

Gene	Log_2 fold change 4 dpi	
	Static 2D PUUV *vs.* mock	Vessel-on-chip PUUV *vs.* mock
Immune response[a]		
IDO1	4.59	7.89
LGALS3BP	5.28	5.73
HLA-F	4.39	5.13
SAMD9	3.75	4.16
HLA-B	3.51	3.96
SAMD9L	3.57	3.69
CFB	2.75	3.55
TLR3	2.90	3.54
SAMHD1	3.13	3.52
SECTM1	2.57	3.31
Chemokines/cytokines		
CXCL10	10.21	8.61
CCL5	4.69	7.81
CXCL11	5.38	5.74
CXCL9	4.92	5.32
TNFSF13B	3.10	3.67
Cell surface markers		
LGALS9B	2.94	4.78
LGALS9	2.39	3.68
LY6E	2.15	2.75
Interferon signaling[a]		
MX2	8.82	8.32
RSAD2	8.00	7.89
CMPK2	6.96	7.57
OASL	5.50	6.16
IFI44L	5.54	5.91
IFITM1	4.52	5.80
RTP4	5.38	5.65

Gene expressions are expressed as log_2 fold change over mock condition of each culturing platform at 4 days post-infection (dpi), ranked on fold change in vessels-on-chip with a cut-off of 2 log_2. [a] Indicates that only top 10 genes are displayed.

Table 2 Unique significantly upregulated genes upon PUUV infection in static 2D- and vessel-on-chip-cultured ECs

Gene	Log_2 fold change 4 dpi	
	Static 2D PUUV *vs.* mock	Vessel-on-chip PUUV *vs.* mock
Immune response		
NEURL3		4.37
C3AR1		3.50
NOD2		1.86
C1R		1.28
BNT3A2		1.15
MR1		1.13
IL1RL1		1.11
TLR6	2.33	
Chemokines/cytokines		
IL7		5.07
CCL23		1.41
IL15		1.28
IL6		1.11
CXCL5	2.74	
EBI3	2.32	
GDF7	2.08	
CCL2	1.91	
Cell surface markers		
IL12RB1		4.61
CD7		3.10
IL7R		1.78
CCRL2		1.38
VSIR		1.00
SELE	1.96	
VCAM1	1.80	
CD164	1.18	
CD34	1.12	
ICAM1	1.02	
Interferon signaling		
IFNB1		8.26
IRF1		1.21
TRIM26		1.15
MOV10		1.15
TRIM5		1.13
Coagulation		
PLAT		1.53
SERPINB2		1.31
SERPIND1		1.21

Gene expressions are expressed as log_2 fold change over mock condition of each culturing platform at 4 days post-infection (dpi).

most significantly enriched pathways in response to PUUV infection in the vessels-on-chip were predominantly involved in regulation of leukocytes, while the top five uniquely enriched pathways under static 2D conditions were mainly enriched for downregulated genes related to vascular transport and biosynthesis.

In conclusion, PUUV infection resulted in anti-viral responses in ECs cultured in both culture models with altered expression of overlapping genes. However, the host response to PUUV infection in vessels-on-chip demonstrated a closer similarity in gene expression of disease markers in patients, such as IDO, Gal-3BP, IL-6, and genes involved in coagulopathy such as *PLAT*, which encodes tissue-type plasminogen activator (tPA). Uniquely enriched pathways during PUUV infection in vessels-on-chip were involved in endothelial-leukocyte interactions. These interactions were based on expression of different immune mediators, chemokines, cytokines and cell surface markers, rather than classic endothelial leukocyte adhesion markers as these were solely upregulated in static 2D cultures and not in vessels-on-chip.

PUUV infection leads to increased leukocyte recruitment in vessels-on-chip

As pathway enrichment analyses upon PUUV infection in vessels-on-chip identified pathways suggesting leukocyte involvement and recruitment, this model was used to investigate the interactions between monocytes and ECs in vessels-on-chip. Primary CD14+ monocytes were added at 4 dpi to vessels-on-chip that were mock-, UV-PUUV- or PUUV-infected. As a positive control for EC-induced monocyte recruitment, vessels-on-chip were treated with TNFα for 24 hours prior to co-incubation. The number of monocytes that adhered to the ECs were imaged (Fig. 4A) and quantified (Fig. 4B). As a result, the number of monocytes adhered to PUUV-infected ECs increased almost 2-fold compared to

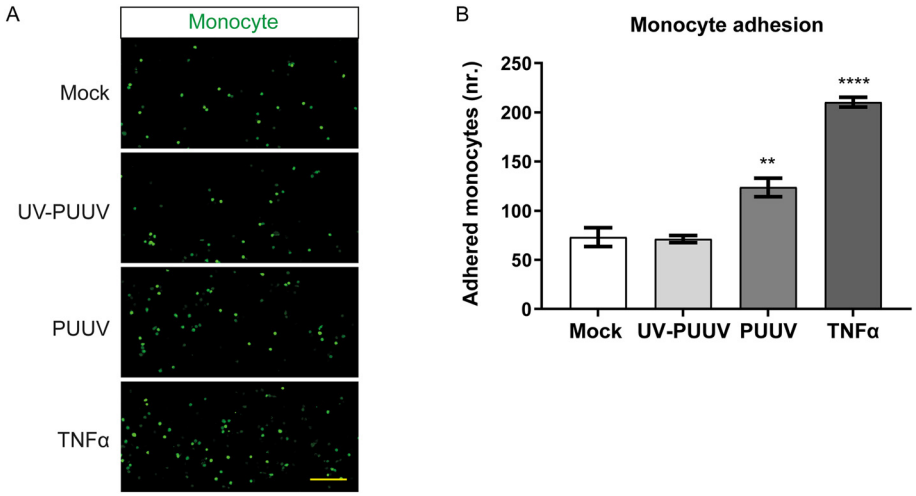

Fig. 4 Monocyte adhesion in vessels-on-chip. (A) Calcein-AM-labeled monocytes were co-cultured for 30 minutes in mock-, UV-PUUV-, PUUV-, and TNFα-treated vessels at 4 days post-infection (dpi). After washing away of non-adhered monocytes, immunofluorescence images were taken. Scale bars indicate 100 μm. (B) Quantification of the number (nr.) of adhered monocytes. Bars represent mean and error bars standard error of the mean. Significant differences were tested by one-way ANOVA with Dunnett's correction by comparing each condition to mock. Results are representative for three independent experiments with each 4 vessels per condition. $^{**}p < 0.005$, $^{****}p < 0.0001$.

mock-infected ECs. Viral replication seemed to be required for this observation as UV-PUUV did not cause any difference in monocyte adhesion. An approximate 3-fold increase in adhering monocytes to TNFα-treated ECs was observed compared to the mock control. Overall, PUUV infection led to increased monocyte adhesion to ECs, which depended on active viral replication.

Discussion

In this study, we aimed to investigate PUUV pathogenesis in ECs in a physiologically relevant culture model. We cultured ECs in a high-throughput vessel-on-chip model, thereby allowing ECs to grow into 3D tube-like architectures of blood vessels with cell densities and area to volume ratios more closely resembling physiological conditions than typical static 2D cultures.[20] These vessels-on-chip were comparable to venules in size and ECs were exposed to *in vivo* levels of shear stress (1–5 dyne per cm^2) with constant exposure to a collagen-1-based ECM gel, which promotes angiogenesis and tube formation.[16,29] These circumstances, especially prolonged exposure to flow,[7] allowed the phenotype of these ECs to more closely resemble the *in vivo* phenotype compared to static 2D EC culture methods lacking flow. In line with our findings, limited inflammatory responses to TNFα by vessels-on-chip, compared to static 2D EC cultures, better resembled the human situation as described before in similar vessels-on-chip models and *ex vivo* cultures of aortic segments.[20,22] To date, this vessel-on-chip platform has been used to study the effects on cytokine-induced increased vascular permeability,[16] metabolic responses[20] and endothelial-leukocyte interactions.[19] Although Ebola and Lassa virus-like particles were used to study effects of viral particles,[30,31] this model has so far not been applied in the context of virus infection. In this study, we demonstrated that this vessel-on-chip model is a valuable tool that allows for the study of EC responses to virus infection. We demonstrated that PUUV infection caused upregulation of genes encoding two known severity of disease immune markers, namely *IDO1*, which encodes IDO,[23] and *LGALS3BP*, which encodes Gal-3BP[24] in ECs. Additionally, in vessels-on-chip gene expression of another known marker of disease severity was upregulated, namely *IL6*, encoding IL-6.[25,26] Also, genes involved in IFN signaling, such as *IFNB1*, *IRF1*, *TRIM26* and genes associated to coagulation, such as *PLAT*, *SERPINB2*, and *SERPIND1*, were upregulated in PUUV-infected vessels-on-chip, which are important findings related to commonly observed coagulopathy in NE patients in clinical settings.[27,28]

In our vessels-on-chip, PUUV infection did not directly impact vascular permeability. Most *in vitro* observations of increased vascular permeability by other orthohantaviruses depended on high concentrations of exogenous vascular endothelial growth factor (VEGF) following starvation of static 2D-cultured ECs, which does not recapitulate pathophysiological conditions during infection.[2,3] As we did not observe increased vascular permeability directly following PUUV infection, an alternative hypothesis suggests that vascular permeability increases *in vivo* are the indirect result of immune-mediated pathology caused by increased robust cytotoxic immune cell responses and immune-derived factors, such as pro-inflammatory cytokines.[25,26,32–38] In line with this hypothesis, we identified interactions with immune cells as the most enriched process uniquely following PUUV infection in vessels-on-chip. We also observed increased monocyte adherence to ECs following PUUV infection in these vessels. So, addition of immune cells to the vessel-on-chip system might be crucial to study the involvement of all components resulting in orthohantavirus-induced EC

activation, leading to immune-driven pathological manifestations, such as increased vascular permeability.

A clinically relevant observation in NE patients is that monocytes translocate from the circulation to affected organs, resulting in an initial loss from circulation during acute disease.[37,39] A previous study identified an upregulation of endothelial adhesion marker L-selectin (CD62L) on monocytes in PUUV patients and proposed a role for L-selectin-mediated adhesion to PUUV-infected ECs as explanation for the initial loss of monocytes from circulation.[37] Importantly, L-selectin-mediated leukocyte adhesion processes should be investigated in presence of physiologically relevant levels of shear stress.[40] Although this condition was met in our vessels-on-chip, we did not detect PUUV-induced upregulation of endothelial L-selectin ligands such as glycosylation-dependent cell adhesion molecule 1 (GlyCAM-1), CD34, mucosal vascular addressin cell adhesion molecule 1 (MAdCAM-1) and P-selectin glycoprotein ligand 1 (PSGL-1) based on RNA-Seq. This suggests that EC responses to PUUV infection *in vivo* might be more complex including more important roles for other factors that have so far been understudied.

An example of these factors identified by RNA-Seq in our study includes *LGALS9*, encoding galectin-9, which was proposed as an adhesion molecule for monocytes,[41] was also upregulated during infection by different orthohantaviruses in HUVECs,[42] and together with Gal-3BP, was also increased in patients suffering from another hemorrhagic fever virus infection; dengue virus.[43,44] Other examples include multiple ligands of the leukocyte chemokine receptor CXCR3, such as *CXCL9*, *CXCL10*, *CXCL11*, and *CCL5*, an important ligand for CCR5, which were all upregulated in response to PUUV infection. This combination of chemokines can be chemotactic for immune cells such as monocytes, activated T cells, B cells and natural killer cells,[45,46] thereby emphasizing once more that future studies should include immune cells in addition to the current vessel-on-chip model to better recapitulate orthohantavirus pathogenesis.

A limitation of the current vessel-on-chip model is that it only supports bidirectional flow, whereas the *in vivo* vasculature is characterized by a continuous, unidirectional flow. This prevents the ECs to align with the direction of such unidirectional flow.[16] However, a previous study demonstrated that within a similar vessel-on-chip model bidirectional flow greatly contributed to elevated expression and improved localization of junctional proteins, and overall vascular barrier integrity as compared to static conditions.[47] In addition, as this gravity-based flow generation does not require a pump system, it can be utilized even in high biocontainment facilities without the need for specialized equipment. Another limitation of the current model is the use of HUVEC monocultures. Although this vessel-on-chip model allows for the study of ECs in a more physiologically relevant context, other relevant cell types associated with the human vasculature including pericytes and smooth muscle cells, could even further improve the translational potential of the model. While HUVECs are the gold standard for research into EC responses and the use of primary pooled HUVECs prevented major donor-specific variations in our current findings, more relevant organ-specific lung- or kidney-derived ECs most likely would improve recapitulation of organ-specific microenvironments.[48] The potential for use of organ-specific ECs also demonstrates the substantial value of this vessel-on-chip platform for pathogenesis studies of various viruses, such as organ-specific endothelial dysfunction following flavivirus nonstructural protein 1 (NS1) stimulation of ECs from different organs.[49,50]

In conclusion, vessel-on-chip cultures provide improved, physiologically relevant conditions to enable the study of ECs that more closely mimic *in vivo* responses, compared to static 2D culture models. In this vessel-on-chip model, PUUV infection did not directly increase vascular permeability, but did lead to increased monocyte adhesion. As demonstrated by RNA-Seq, this model represents a valuable tool to study endothelial-leukocyte interactions in the context of PUUV infection. The model allows for high-throughput studies and does not require the usage of pumps, which makes this platform very appealing to be used for a whole range of infectious agents, including at BSL-3 and BSL-4. Therefore, it can be applied for pathogenesis studies and screens for potential prophylactic or therapeutic interventions of orthohantaviruses and other infectious agents affecting the vasculature.

Methods

Cells

Primary pooled human umbilical vein endothelial cells (HUVECs; PromoCell) were cultured in endothelial cell (EC) growth medium MV2 (PromoCell) supplemented with 100 IU mL^{-1} penicillin and 100 μg mL^{-1} streptomycin (Lonza). Tissue culture flasks were pre-coated with 1% gelatin (Sigma) prior to HUVECs culture. HUVECs were used up to passage 10. For virus propagation, Vero E6 cells (CRL-1586, ATCC) were cultured in Dulbecco's modified Eagle medium (DMEM, Lonza) supplemented with 10% fetal calf serum (FCS), HEPES, sodium bicarbonate, 100 IU mL^{-1} penicillin and 100 μg mL^{-1} streptomycin (Lonza). All cells were cultured in a humidified incubator at 37 °C, 5% CO_2. Medium was refreshed 2–3 times per week. All cells and virus stocks were confirmed to be negative for presence of mycoplasma.

Vessel-on-chip and static two-dimensional endothelial cell culture

For three-dimensional (3D) microfluidic endothelial vessel-on-chip culture, the OrganoPlate 2-lane culture platform (9605–400-B, Mimetas) was used. Prior to gel loading, observation wells were filled with 70 μL phosphate-buffered saline (PBS) to enhance optical clarity. The extracellular matrix (ECM) gel was prepared by mixing 5 mg mL^{-1} rat collagen-I (Sigma), 1 M HEPES, and 37 g L^{-1} $NaHCO_3$ (in sterile milliQ pH = 9.0, Sigma) in an 8 : 1 : 1 ratio. In every gel inlet well, 1.8 μL of ECM gel was loaded and placed in a humidified incubator (37 °C and 5% CO_2) for 10 minutes

to allow polymerization of the ECM gel. Subsequently, the perfusion channel of each chip was coated with 70 μL 1% gelatin coating solution added to the perfusion outlet wells, *i.e.* the most right well of each chip, and the plate was further incubated in a humidified incubator. Two to three days later, ECs were trypsinized, harvested and collected from tissue culture flasks. ECs were resuspended in EC culture medium to obtain a concentration of 2.0×10^7 cells per mL. In the chips, gelatin coating solution was aspirated from the perfusion outlet wells. Directly after, 25 μL of EC culture medium was added to the perfusion outlet wells, and 1 μL of cell suspension was added to each perfusion inlet well, *i.e.* the well closest to the gel inlet well. This resulted in 2.0×10^4 cells per chip evenly distributed along the perfusion channel. The plate was placed into a humidified incubator for 1.5 hours to allow adherence of ECs to the bottom of the perfusion channel. After ECs were attached, the medium in the perfusion outlet well was aspirated and 50 μL of fresh EC culture medium was added to both the perfusion inlet and outlet wells. The device was placed on an interval rocker platform (Mimetas) set at a 7 degree inclination and 8 minute cycle time for interval perfusion. Medium was refreshed every two days. In parallel to vessel-on-chip culture, ECs collected from the same tissue culture flasks were cultured under static two-dimensional (2D) conditions, *i.e.* in 96-wells plates (Greiner) without the use of the rocking platform, hence lacking flow. Similar to vessel-on-chip culture, 1% gelatin coating solution was added to each well. Two to three days later, ECs were also seeded at 2.0×10^4 cells per well and placed into a humified incubator and medium was refreshed every two days. This seeding approach allowed for direct comparison of EC responses as in both models each chip or well contained approximately 4.0×10^4 cells at the start of experiments.

Virus infections and quantification

Puumala orthohantavirus strain Cg 18–20 (PUUV, European Virus Archive Global #007v-00809, P+3) stocks were propagated on Vero E6 cells, as described for Seoul orthohantavirus.[51] Virus stock titers were quantified by 50% tissue culture infectious dose ($TCID_{50}$) dilution assays. Replication-incompetent PUUV (UV-PUUV) stocks were freshly generated prior to every infection experiment by UV-irradiation (2.4 J cm^{-2} at 254 nm, Avantor). Successful UV-inactivation was confirmed by quantitative reverse transcription polymerase chain reaction (RT-qPCR). For determining virus replication kinetics, infections were performed by inoculating ECs for two hours with PUUV, UV-PUUV or mock infection, *i.e.* identical volume of Vero E6 cell culture medium diluted in EC culture medium as during inoculation with infectious PUUV stock. ECs were infected at a multiplicity of infection (MOI) of 1.0. Two hours post-infection, cells were washed three times with PBS and 100 μL fresh EC culture medium was added to each chip or well. EC culture medium was refreshed every two days and 60 μL of supernatant was collected to monitor virus replication kinetics and stored at −80 °C until RNA isolation. Prior to RT-qPCR, a known concentration of phocine distemper virus (PDV) was added to each sample as internal control for RNA isolation.[52] RNA isolation was performed as described with the modification that RNA was eluted in 30 μl PCR grade water.[53] PUUV RNA was amplified with in-house designed Taqman primer-probe sets targeting the small (S) segment of PUUV including forward primer 5'AGGCAACAAACAGTGTCAG CA-3′, reverse primer 5′-GCATTTACATCAAGGACATTTCCATA-3′, and FAM/BHQ1-labeled probe 5′-CTGACCCGACTGGGATTGAAC CTGATG-3′ on a 7500 real-time PCR system (Applied Biosystems). Ct-values were converted to $TCID_{50}$ equivalents per mL by comparison to standard curves from PUUV stocks titrated on Vero E6 cells that were included during each round of RT-qPCR.

Vessels-on-chip vascular permeability assay

To characterize the vascular permeability of vessels-on-chip, medium was removed from the pefusion channel. Then, 20 μL of EC culture medium was dispensed in the gel inlet well. After which, 40 and 30 μL of a mixture of fluorescently-labeled dextrans consisting of 20 kDa-Cy5 (Nanocs) or 20 kDa-FITC (Sigma) with 155 kDa-TRITC (Sigma) at a concentration of 0.125 mg mL^{-1} diluted in EC culture medium were introduced to the perfusion in- and outlet well, respectively. Ten minutes after addition of the dextran mixture, dextran translocations were visualized by acquiring the fluorescence intensity of the perfusion channel (I_{vessel}) and the ECM channel (I_{ECM}) (Fig. 1A and D) every two minutes for ten minutes total using a LSM700 confocal microscope using ZEN software (Zeiss). Fluorescence intensity was quantified for manually defined regions of interest (ROIs) for the perfusion channel and the gel channel using ImageJ software (NIH).[54] The translocation of fluorescently-labeled dextran reporters was normalized by the surface area of the vessel in contact with the ECM, and the volume of the gel. The apparent permeability (P_{app}) was calculated, based on a previous study,[16] in short: $P_{app}\left(\text{cm s}^{-1}\right) = \frac{\mathrm{d}\left(\frac{I_{ECM}}{I_{Vessel}}\right)}{\mathrm{d}t} \times \frac{V_{ECM}}{A}$ where I_{ECM}/I_{Vessel} is the ratio of intensity between the ECM and perfusion channel with V_{ECM} the volume of the ECM (7.43×10^{-4} cm^3), and A the surface area of the vessel wall between the ECM and vessel (2.08×10^{-2} cm^2). The ratio (I_{ECM}/I_{vessel}) was calculated for each individual time point. This calculation results in the change in fluorescence intensity ratio inside the ECM channel as a function over time. To establish on which days post-seeding (dps) the vessels-on-chip formed an optimal and stable barrier, the P_{app} was calculated on different dps and compared to maximum P_{app} represented by the intrinsic barrier of the ECM gel in absence of ECs, *i.e.* no cells. Incidentally, vessels were excluded based on morphological malformation in vessel structure as assessed by light microscopy. As positive

controls for increased vascular permeability, vessels were stimulated with 100 ng mL^{-1} tumor necrosis factor alpha (TNFα) 24 hours prior to the vascular permeability assay. Perfusion inlet and outlet wells were aspirated and 50 μL of stimulus in EC culture medium was added to both the perfusion inlet and outlet wells. After image acquisition, vessels were either refreshed with EC culture medium or fixed for subsequent immunofluorescence staining.

Immunofluorescence staining

To visualize viral antigen or cell markers, ECs were washed three times with EC culture medium or two times directly after the vascular permeability assay to keep similar conditions, *i.e.* three times flushing with EC culture medium before fixation. ECs were fixed with 4% neutral-buffered formalin, in case of the vessels-on-chip under an angle to create flow and stimulate penetration of all sides of the vessels. After 30 minutes of fixation, cells were washed twice with PBS to remove fixative, and cells were permeabilized for 5 minutes with 70% ethanol after which cells were washed once with PBS. From this step onwards, the microfluidic plate was no longer placed under an angle, while static 2D-cultured ECs were fixed and permeabilized without an angle. Cells were blocked with 5% bovine serum albumin (BSA, Sigma) for 1 hour at room temperature followed by one PBS wash. Cells were incubated overnight at 4 °C with primary antibody mix in 1% BSA diluted in PBS. Primary antibodies used were goat polyclonal anti-VE-cadherin antibody (1 : 20, RnD Systems), mouse monoclonal anti-CD31 antibody (1 : 100, Agilent), mouse monoclonal anti-Von Willebrand factor (vWF) antibody (1 : 100, Invitrogen), and rabbit polyclonal anti-PUUV nucleocapsid (PUUV N) IgG (1 : 500, BEI Resources, NIAID, NIH). After two washes with PBS, secondary antibody mix in 1% BSA in PBS was applied for 1 hour at room temperature. Secondary antibodies used were Alexa Fluor 488-conjugated donkey anti-mouse IgG antibody (1 : 500, Invitrogen), Alexa Fluor 488-conjugated donkey anti-rabbit IgG antibody (1 : 500, Invitrogen), Alexa Fluor 555-conjugated donkey anti-goat IgG antibody (1 : 500, Invitrogen) and Alexa Fluor 647-conjugated donkey anti-goat IgG antibody (1 : 500, Invitrogen). After which, nuclei were visualized with Hoechst 33342 or TO-PRO-3 (Invitrogen) in PBS for 15 minutes. Finally, cells were washed twice with PBS, left in PBS and stored at 4 °C until imaged using a LSM700 confocal microscope. Representative Z-stack images were taken from the monolayer of static 2D cultures or the bottom monolayer of each vessel-on-chip. A 3D render of vessels-on-chip was made using Dragonfly 2022.2 software (Comet Technologies Canada Inc.). This software is available at **https://www.theobjects.com/dragonfly**.

Transcriptomic analyses

ECs that were mock- or PUUV-infected for 4 dpi, or treated with TNFα for 24 hours, were harvested for transcriptomic analysis. Prior to sample collection, vessels-on-chip and static 2D EC cultures were washed once with EC culture medium to remove dead cells. Vessels-on-chip were lysed by applying 10 μL of lysis buffer (Roche) to the gel inlet well, 65 μL to the perfusion inlet well and 25 μL to the perfusion outlet well, creating a flow through the perfusion channel. After 15 minutes, 20, 40 and 40 μL of PBS were added respectively. Lysed cells were collected and five vessels-on-chip were pooled to represent one sample per condition. For static 2D EC cultures, also 100 μL lysis buffer was added to each well with addition of 100 μL of PBS 15 minutes later. Five wells were pooled to represent one sample per condition, resulting in similar number of ECs per sample for both static 2D and vessel-on-chip. Total RNA from these samples was isolated using the high pure RNA isolation kit (Roche) according to manufacturer's guidelines. Prior to transcriptomic analyses, efficient PUUV replication was confirmed *via* RT-qPCR on supernatants as described earlier. Triplicate aliquots per condition were stored at −80 °C and sent out for bulk RNA-sequencing (RNA-Seq) at the Erasmus Center for Biomics.

RNA-Seq library preparation

Total RNA was checked for quality on an Agilent Technologies 2100 Bioanalyzer using a RNA nano assay. All samples had RIN values greater than 8. RNA-Seq libraries were prepared according to the manufacturer's instruction TruSeq stranded mRNA protocol (Illumina). In short, 200 ng of total RNA was purified using poly-T oligo-attached magnetic beads to yield poly-A containing mRNA. The poly-A-tailed mRNA was fragmented and cDNA was synthesized using SuperScript II and random primers in the presence of actinomycin D. The cDNA fragments were end repaired, purified with AMPure XP beads, and A-tailed using Klenow exo-enzyme in the presence of dATP. Paired-end adapters with dual index (Illumina) were ligated to the A-tailed cDNA fragments and purified using AMPure XP beads. The resulting adapter-modified cDNA fragments were enriched by PCR using Phusion polymerase as followed: 30 s at 98 °C, 15 cycles (of 10 s at 98 °C, 30 s at 60 °C, 30 s at 72 °C), 5 min at 72 °C. PCR products were purified using AMPure XP beads and eluted in 30 μL of resuspension buffer. One μL was loaded on an Agilent Technologies 2100 Bioanalyzer using a DNA 1000 assay to determine the library concentration and for quality check. The libraries were sequenced for paired-end reads, 50 bp in length, on NextSeq2000. At least 20 M clusters were generated for each library.

RNA-Seq primary analysis and differential gene expression

AdapterTrimmer was used to trim off Illumina adapter sequences from the reads,[55] which were subsequently mapped against the reference using HiSat2 version 2.2.1.[56] For the libraries, GRCh38 reference genome was used. Gene expression values were called using htseq-count version 0.12.4[57] and the CCDS and mirbase genes from Ensembl release 101 gene and transcript annotation. Sample QC and differential gene expression analysis were performed in the

R environment for statistical computing version 3.6.3,[58] using the packages DESeq2 version 1.26.0,[59] and tidyverse version 1.3.0,[60] and visualized using ggplot and EnhancedVolcano. Significantly upregulated gene expressions were defined as $-\log_{10} P \geq 2$ with $\log_2$ fold change >1 while significantly downregulated gene expressions were defined as $-\log_{10} P \geq 2$ with $\log_2$ fold change < −1. Venn diagrams for significantly differentially expressed genes were created using InteractiVenn.[61] Differentially expressed genes were manually categorized in tables by consulting corresponding gene and encoding protein data in the National Center for Biotechnology Information (NCBI) Gene database[62] and the Human Protein Atlas,[63,64] accessed on March 28th 2024.

Pathway enrichment analyses

The gseGO function from the ClusterProfiler R package version 4.12.0 was used to test for association of the differentially expressed genes with gene ontology gene sets. The gene list of differentially expressed genes was selected using an adjusted *P*-value below 0.01 for all differential expression tests. The gene list was arranged on $\log_2$ fold change.

Monocyte adhesion assay

For experiments involving human buffy coats, written informed consent for research use was obtained by the Sanquin Blood Bank. Peripheral blood mononuclear cells (PBMCs) were isolated from buffy coats from a healthy anonymous blood donor (Sanquin, Rotterdam, the Netherlands). PBMCs were isolated by density centrifugation using Ficoll Paque PLUS (GE Healthcare). Monocytes were magnetically sorted using $CD14^+$ MACS microbeads (Miltenyi Biotec).[65] Monocytes were freshly isolated and added at 4 dpi to vessels-on-chip that were mock-, UV-PUUV- or PUUV-infected, or, as positive control for monocyte recruitment, treated with 100 ng mL^{-1} TNFα for 24 hours prior to co-incubation. The freshly isolated monocytes were stained with calcein-AM (BioLegend) for 20 minutes at room temperature according to manufacturer's instructions. After PBS washing and centrifugation, monocytes were diluted in EC culture medium. Monocytes were incubated at 37 °C, 5% CO_2 to rest for at least 30 minutes prior to the addition to the vessels-on-chip. Subsequently, vessels-on-chip were washed once with EC culture medium, and monocytes were added in a 1 : 10 (EC : monocyte) ratio in 100 μL per vessel and the plate was incubated on a rocking platform (7°, interval 8 minutes) in a 37 °C, 5% CO_2 incubator. After 30 minutes of co-culture, vessels were washed once with EC culture medium and three times with PBS to remove non-adhering monocytes. Finally, vessels were left in PBS and directly imaged using a LSM700 confocal microscope. Monocytes were imaged at 10× magnification and the number of adhered monocytes to the bottom monolayer of each vessel were quantified for equally-sized representative ROIs per vessel-on-chip using ImageJ software.[54]

Statistical analyses

Statistical analyses were performed using GraphPad Prism 10 software and Adobe Illustrator was used to combine data visualizations into final figures. Vascular permeability values for barrier formation optimization on multiple time points were compared to the control condition without cells for each of the dextrans by two-way ANOVA with Dunnett's correction. Vascular permeability values and number of adhering monocytes in treated vessels-on-chip were statistically compared by one-way ANOVA with Dunnett's correction by comparison of each condition to mock. All results were expressed as means with standard error of the mean (SEM) with a *P*-value below 0.05 considered statistically significant.

Data availability

The data supporting the findings of this study are available on NCBI GEO database under accession code GSE270172.

Author contributions

Danny Noack: conceptualization, methodology, investigation, data curation, formal analysis, visualization, writing – original draft, writing – review and editing. Anouk van Haperen data curation, formal analysis, visualization, writing – review and editing. Mirjam C. G. N. van den Hout formal analysis, visualization, writing – review and editing. Eleanor M. Marshall formal analysis, visualization, writing – review and editing. Rosanne W. Koutstaal methodology, writing – review and editing. Vincent van Duinen methodology, writing – review and editing. Lisa Bauer methodology, writing – review and editing. Anton Jan van Zonneveld supervision, writing – review and editing. Wilfred F. J. van IJcken supervision, writing – review and editing. Marion P. G. Koopmans supervision, writing – review and editing. Barry Rockx conceptualization, formal analysis, supervision, writing – review and editing.

Conflicts of interest

The authors report no conflict of interest.

Acknowledgements

The authors thank Fatih Anfasa, Melanie van Heteren-Hemelop, Imke Visser, Stefan van Nieuwkoop, Manou van Alphen (Dept. Viroscience, Erasmus MC, Rotterdam), Bastian Hornung (Dept. Cell Biology, Erasmus MC, Rotterdam) and Marco Goeijenbier (Dept. Intensive Care, Erasmus MC, Rotterdam) for technical advice and scientific discussions. This work was funded in part by the Netherlands Centre for One Health Ph.D. Research Program (**http://www.ncoh.nl**).

References

1 D. Noack, M. Goeijenbier, C. Reusken, M. P. G. Koopmans and B. H. G. Rockx, *Front. Cell. Infect. Microbiol.*, 2020, **10**, 399.
2 I. N. Gavrilovskaya, E. E. Gorbunova, N. A. Mackow and E. R. Mackow, *J. Virol.*, 2008, **82**, 5797–5806.
3 E. Gorbunova, I. N. Gavrilovskaya and E. R. Mackow, *J. Virol.*, 2010, **84**, 7405–7411.
4 P. Shrivastava-Ranjan, P. E. Rollin and C. F. Spiropoulou, *J. Virol.*, 2010, **84**, 11227–11234.
5 S. L. Taylor, V. Wahl-Jensen, A. M. Copeland, P. B. Jahrling and C. S. Schmaljohn, *PLoS Pathog.*, 2013, **9**, e1003470.
6 J. J. Chiu and S. Chien, *Physiol. Rev.*, 2011, **91**, 327–387.
7 Y. Afshar, F. Ma, A. Quach, A. Jeong, H. L. Sunshine, V. Freitas, Y. Jami-Alahmadi, R. Helaers, X. Li, M. Pellegrini, J. A. Wohlschlegel, C. E. Romanoski, M. Vikkula and M. L. Iruela-Arispe, *eLife*, 2023, **12**, e81370.
8 N. Baeyens, C. Bandyopadhyay, B. G. Coon, S. Yun and M. A. Schwartz, *J. Clin. Invest.*, 2016, **126**, 821–828.
9 J. W. Song, J. Daubriac, J. M. Tse, D. Bazou and L. L. Munn, *Lab Chip*, 2012, **12**, 5000–5006.
10 Y. Zheng, J. Chen, M. Craven, N. W. Choi, S. Totorica, A. Diaz-Santana, P. Kermani, B. Hempstead, C. Fischbach-Teschl, J. A. Lopez and A. D. Stroock, *Proc. Natl. Acad. Sci. U. S. A.*, 2012, **109**, 9342–9347.
11 J. A. Jimenez-Torres, S. L. Peery, K. E. Sung and D. J. Beebe, *Adv. Healthcare Mater.*, 2016, **5**, 198–204.
12 E. Akbari, G. B. Spychalski, K. K. Rangharajan, S. Prakash and J. W. Song, *Micromachines*, 2019, **10**(7), 451.
13 C. Mandrycky, B. Hadland and Y. Zheng, *Sci. Adv.*, 2020, **6**(38), eabb3629.
14 A. Jain, A. D. van der Meer, A. L. Papa, R. Barrile, A. Lai, B. L. Schlechter, M. A. Otieno, C. S. Louden, G. A. Hamilton, A. D. Michelson, A. L. Frelinger, 3rd and D. E. Ingber, *Biomed. Microdevices*, 2016, **18**, 73.
15 S. L. N. Brouns, I. Provenzale, J. P. van Geffen, P. E. J. van der Meijden and J. W. M. Heemskerk, *J. Thromb. Haemostasis*, 2020, **18**, 931–941.
16 V. van Duinen, A. van den Heuvel, S. J. Trietsch, H. L. Lanz, J. M. van Gils, A. J. van Zonneveld, P. Vulto and T. Hankemeier, *Sci. Rep.*, 2017, **7**, 18071.
17 E. Yildirim, S. J. Trietsch, J. Joore, A. van den Berg, T. Hankemeier and P. Vulto, *Lab Chip*, 2014, **14**, 3334–3340.
18 V. van Duinen, W. Stam, V. Borgdorff, A. Reijerkerk, V. Orlova, P. Vulto, T. Hankemeier and A. J. van Zonneveld, *J. Visualized Exp.*, 2019, **153**, e59678.
19 C. Poussin, B. Kramer, H. L. Lanz, A. Van den Heuvel, A. Laurent, T. Olivier, M. Vermeer, D. Peric, K. Baumer, R. Dulize, E. Guedj, N. V. Ivanov, M. C. Peitsch, J. Hoeng and J. Joore, *ALTEX*, 2020, **37**, 47–63.
20 A. Junaid, J. Schoeman, W. Yang, W. Stam, A. Mashaghi, A. J. van Zonneveld and T. Hankemeier, *eLife*, 2020, **9**, e54754.
21 J. Surapisitchat, R. J. Hoefen, X. Pi, M. Yoshizumi, C. Yan and B. C. Berk, *Proc. Natl. Acad. Sci. U. S. A.*, 2001, **98**, 6476–6481.
22 H. Yamawaki, S. Lehoux and B. C. Berk, *Circulation*, 2003, **108**, 1619–1625.
23 T. K. Outinen, S. M. Makela, I. O. Ala-Houhala, H. S. Huhtala, M. Hurme, D. H. Libraty, S. S. Oja, I. H. Porsti, J. T. Syrjanen, A. Vaheri and J. T. Mustonen, *J. Med. Virol.*, 2011, **83**, 731–737.
24 J. Hepojoki, T. Strandin, U. Hetzel, T. Sironen, J. Klingstrom, J. Sane, S. Makela, J. Mustonen, S. Meri, A. Lundkvist, O. Vapalahti, H. Lankinen and A. Vaheri, *J. Gen. Virol.*, 2014, **95**, 2356–2364.
25 M. Linderholm, C. Ahlm, B. Settergren, A. Waage and A. Tarnvik, *J. Infect. Dis.*, 1996, **173**, 38–43.
26 T. K. Outinen, S. M. Makela, I. O. Ala-Houhala, H. S. Huhtala, M. Hurme, A. S. Paakkala, I. H. Porsti, J. T. Syrjanen and J. T. Mustonen, *BMC Infect. Dis.*, 2010, **10**, 132.
27 T. Strandin, J. Hepojoki, O. Laine, S. Makela, J. Klingstrom, A. Lundkvist, I. Julkunen, J. Mustonen and A. Vaheri, *J. Infect. Dis.*, 2016, **213**, 1632–1641.
28 C. Bellomo, M. Korva, A. Papa, S. Makela, J. Mustonen, T. Avsic-Zupanc, A. Vaheri, V. P. Martinez and T. Strandin, *Open Forum Infect. Dis.*, 2018, **5**, ofy021.
29 Y. Liu and D. R. Senger, *FASEB J.*, 2004, **18**, 457–468.
30 A. Junaid, H. Tang, A. van Reeuwijk, Y. Abouleila, P. Wuelfroth, V. van Duinen, W. Stam, A. J. van Zonneveld, T. Hankemeier and A. Mashaghi, *iScience*, 2020, **23**, 100765.
31 H. Tang, Y. Abouleila and A. Mashaghi, *Biotechnol. Bioeng.*, 2021, **118**, 1405–1410.
32 T. Lindgren, C. Ahlm, N. Mohamed, M. Evander, H. G. Ljunggren and N. K. Bjorkstrom, *J. Virol.*, 2011, **85**, 10252–10260.
33 M. Sadeghi, I. Eckerle, V. Daniel, U. Burkhardt, G. Opelz and P. Schnitzler, *BMC Immunol.*, 2011, **12**, 65.
34 M. Braun, N. K. Bjorkstrom, S. Gupta, K. Sundstrom, C. Ahlm, J. Klingstrom and H. G. Ljunggren, *PLoS Pathog.*, 2014, **10**, e1004521.
35 J. Rasmuson, J. Pourazar, N. Mohamed, K. Lejon, M. Evander, A. Blomberg and C. Ahlm, *Eur. J. Clin. Microbiol. Infect. Dis.*, 2016, **35**, 713–721.
36 S. F. Khaiboullina, S. Levis, S. P. Morzunov, E. V. Martynova, V. A. Anokhin, O. A. Gusev, S. C. St Jeor, V. C. Lombardi and A. A. Rizvanov, *Front. Immunol.*, 2017, **8**, 567.
37 S. Vangeti, T. Strandin, S. Liu, J. Tauriainen, A. Raisanen-Sokolowski, L. Cabrera, A. Hassinen, S. Makela, J. Mustonen, A. Vaheri, O. Vapalahti, J. Klingstrom and A. Smed-Sorensen, *PLoS Pathog.*, 2021, **17**, e1009400.
38 D. Noack, M. Travar, V. Mrdjen, J. J. C. Voermans, D. van de Vijver, R. Molenkamp, M. P. G. Koopmans, M. Goeijenbier and B. Rockx, *Viruses*, 2022, **14**(7), 1377.
39 S. Scholz, F. Baharom, G. Rankin, K. T. Maleki, S. Gupta, S. Vangeti, J. Pourazar, A. Discacciati, J. Hoijer, M. Bottai, N. K. Bjorkstrom, J. Rasmuson, M. Evander, A. Blomberg, H. G. Ljunggren, J. Klingstrom, C. Ahlm and A. Smed-Sorensen, *PLoS Pathog.*, 2017, **13**, e1006462.
40 E. B. Finger, K. D. Puri, R. Alon, M. B. Lawrence, U. H. von Andrian and T. A. Springer, *Nature*, 1996, **379**, 266–269.
41 F. Krautter, M. T. Hussain, Z. Zhi, D. R. Lezama, J. E. Manning, E. Brown, N. Marigliano, F. Raucci, C. Recio, M. Chimen, F. Maione, A. Tiwari, H. M. McGettrick, D. Cooper, E. A. Fisher and A. J. Iqbal, *Atherosclerosis*, 2022, **363**, 57–68.

42 E. Geimonen, S. Neff, T. Raymond, S. S. Kocer, I. N. Gavrilovskaya and E. R. Mackow, *Proc. Natl. Acad. Sci. U. S. A.*, 2002, **99**, 13837–13842.
43 H. Chagan-Yasutan, L. C. Ndhlovu, T. L. Lacuesta, T. Kubo, P. S. Leano, T. Niki, S. Oguma, K. Morita, G. M. Chew, J. D. Barbour, E. F. Telan, M. Hirashima, T. Hattori and E. M. Dimaano, *J. Clin. Virol.*, 2013, **58**, 635–640.
44 K. T. Liu, Y. H. Liu, Y. H. Chen, C. Y. Lin, C. H. Huang, M. C. Yen and P. L. Kuo, *Int. J. Mol. Sci.*, 2016, **17**(6), 832.
45 D. D. Taub, A. R. Lloyd, K. Conlon, J. M. Wang, J. R. Ortaldo, A. Harada, K. Matsushima, D. J. Kelvin and J. J. Oppenheim, *J. Exp. Med.*, 1993, **177**, 1809–1814.
46 S. Qin, J. B. Rottman, P. Myers, N. Kassam, M. Weinblatt, M. Loetscher, A. E. Koch, B. Moser and C. R. Mackay, *J. Clin. Invest.*, 1998, **101**, 746–754.
47 N. R. Wevers, D. G. Kasi, T. Gray, K. J. Wilschut, B. Smith, R. van Vught, F. Shimizu, Y. Sano, T. Kanda, G. Marsh, S. J. Trietsch, P. Vulto, H. L. Lanz and B. Obermeier, *Fluids Barriers CNS*, 2018, **15**, 23.
48 S. K. H. Morsing, E. Zeeuw van der Laan, A. D. van Stalborch, J. D. van Buul, A. P. J. Vlaar and R. Kapur, *Physiol. Rep.*, 2022, **10**, e15271.
49 H. Puerta-Guardo, D. R. Glasner, D. A. Espinosa, S. B. Biering, M. Patana, K. Ratnasiri, C. Wang, P. R. Beatty and E. Harris, *Cell Rep.*, 2019, **26**, 1598–1613 e1598.
50 A. B. Haymet, N. Bartnikowski, E. S. Wood, M. P. Vallely, A. McBride, S. Yacoub, S. B. Biering, E. Harris, J. Y. Suen and J. F. Fraser, *Front. Cardiovasc. Med.*, 2021, **8**, 647086.
51 D. Noack, M. van den Hout, C. W. E. Embregts, I. W. F. J. van, M. P. G. Koopmans and B. Rockx, *PLoS Neglected Trop. Dis.*, 2024, **18**, e0012074.
52 G. J. van Doornum, M. Schutten, J. Voermans, G. J. Guldemeester and H. G. Niesters, *J. Med. Virol.*, 2007, **79**, 1868–1876.
53 R. D. de Vries, K. S. Schmitz, F. T. Bovier, C. Predella, J. Khao, D. Noack, B. L. Haagmans, S. Herfst, K. N. Stearns, J. Drew-Bear, S. Biswas, B. Rockx, G. McGill, N. V. Dorrello, S. H. Gellman, C. A. Alabi, R. L. de Swart, A. Moscona and M. Porotto, *Science*, 2021, **371**, 1379–1382.
54 C. A. Schneider, W. S. Rasband and K. W. Eliceiri, *Nat. Methods*, 2012, **9**, 671–675.
55 *GitHub, Inc. AdapterTrimmer*, (URL: **https://www.github.com/erasmus-center-for-biomics/AdapterTrimmer**).
56 D. Kim, B. Langmead and S. L. Salzberg, *Nat. Methods*, 2015, **12**, 357–360.
57 S. Anders, P. T. Pyl and W. Huber, *Bioinformatics*, 2015, **31**, 166–169.
58 *R Core Team*, R: A language and environment for satistical computing, (URL: **http://www.R-project.org**).
59 M. I. Love, W. Huber and S. Anders, *Genome Biol.*, 2014, **15**, 550.
60 *GitHub, Inc. Tidyverse*, (URL: **https://www.github.com/tidyverse**).
61 H. Heberle, G. V. Meirelles, F. R. da Silva, G. P. Telles and R. Minghim, *BMC Bioinf.*, 2015, **16**, 169.
62 G. R. Brown, V. Hem, K. S. Katz, M. Ovetsky, C. Wallin, O. Ermolaeva, I. Tolstoy, T. Tatusova, K. D. Pruitt, D. R. Maglott and T. D. Murphy, *Nucleic Acids Res.*, 2015, **43**, D36–42.
63 *Human Protein Atlas*, (URL: **https://www.proteinatlas.org**).
64 M. Uhlen, P. Oksvold, L. Fagerberg, E. Lundberg, K. Jonasson, M. Forsberg, M. Zwahlen, C. Kampf, K. Wester, S. Hober, H. Wernerus, L. Bjorling and F. Ponten, *Nat. Biotechnol.*, 2010, **28**, 1248–1250.
65 C. W. E. Embregts, A. S. Wentzel, A. T. den Dekker, I. W. F. J. van, R. Stadhouders and C. H. GeurtsvanKessel, *Front. Cell. Infect. Microbiol.*, 2023, **13**, 1013842.